

Colliding interstellar bubbles in the direction of $l = 54^\circ$

L. Zychová¹ and S. Ehlerová²

¹ Department of Theoretical Physics and Astrophysics, Faculty of Science, Masaryk University, Kotlářská 2, 611 37 Brno, Czech Republic

² Astronomical Institute, Academy of Sciences of the Czech Republic, Boční II 1401, 141 31 Prague 4, Czech Republic

Received December 4, 2015; accepted August 30, 2016

ABSTRACT

Context. Interstellar bubbles are structures in the interstellar medium with diameters of a few to tens of parsecs. Their progenitors are stellar winds, intense radiation of massive stars, or supernova explosions. Star formation and young stellar objects are commonly associated with these structures.

Aims. We compare IR observations of bubbles N115, N116 and N117 with atomic, molecular and ionized gas in this region. While determining the dynamical properties of the bubbles, we also look into their ambient environment to understand their formation in a wider context.

Methods. For finding bubbles in HI (VLA Galactic Plane Survey) and CO data (Galactic Ring Survey), we used their images from Galactic Legacy Infrared Mid-Plane Survey. We manually constructed masks based on the appearance of the bubbles in the IR images and applied it to the HI and CO data. We determined their kinematic distance, size, expansion velocity, mass, original density of the maternal cloud, age and energy input.

Results. We identified two systems of bubbles: the first, background system, is formed by large structures G053.9+0.2 and SNR G054.4-0.3 and the infrared bubble N116+117. The second, foreground system, includes the infrared bubble N115 and two large HI bubbles, which we discovered in the HI data. Both systems are independent, lying at different distances, but look similar. They are both formed by two large colliding bubbles with radii around 20–30 pc and ages of a few million years. A younger and smaller (~4 pc, less than a million years) infrared bubble lies at the position of the collision.

Conclusions. We found that both infrared bubbles N115 and N116+117 are associated with the collisions of larger and older bubbles. We propose, that such collisions increase the probability of further star formation, probably by squeezing the interstellar material, suggesting that it is an important mechanism for star formation.

Key words. ISM: bubbles – ISM: clouds – ISM: HII regions – ISM: supernova remnants

1. Introduction

1.1. Interstellar bubbles

The interstellar medium (ISM) in the Galaxy shows a rich variety of structures, including clumps, filaments and dense sheets. Some of the structures resemble envelopes and are known as shells or bubbles. Their (nearly) ubiquitous presence is the reason behind the term “the bubbling galactic disk” (Churchwell et al. 2006; Deharveng et al. 2010; Simpson et al. 2012), describing the state of the ISM. Progenitors of these bubbles, which are best observable in the infrared band, include stellar winds, intense radiation of massive stars, or supernova explosions. Basically all infrared (IR) bubbles are found near HII regions, CO clouds or other indicators of the recent or on-going star formation.

The walls delineating the IR bubbles are associated with sites of the new star formation, i.e. they contain objects younger than the predicted age of the bubble itself – many examples can be found in (Deharveng et al. 2010), suggesting triggered star formation. There are two basic mechanisms proposed to explain such triggering: Collect & Collapse (C&C) and Radiation Driven Implosion (RDI). In the first one, the interstellar medium is swept up into a dense cold layer and this layer gravitationally fragments and then forms stars. In the second scenario the shock front compresses existing cold clumps and thus initiates the star formation.

It is difficult to distinguish between these scenarios (see, e.g. Walch et al. 2015, for the discussion of these questions connected with the IR bubble RCW 120), and there is still the possibility that no real triggering is taking place, just shifting and relocation of material, which would also form stars without any external driver (see Dale et al. 2015, for a discussion about what triggering really means).

In this paper, we compare the IR observations of bubbles N115, N116 and N117 from Churchwell et al. (2006) with atomic (HI), molecular (CO) and ionized (radio continuum) gas in this region. We find two independent subsystems, which both look very much alike: colliding bubbles with the star formation taking place in the position of the collision. In the following section we first summarize what is known about the studied bubbles and then we describe the data and the methods of the analysis. Afterwards, we will describe each subsystem separately and calculate its properties. We conclude the paper with a brief discussion.

1.2. The region around infrared bubbles N115, N116 and N117

Infrared bubbles N115, N116 and N117 were identified by Churchwell et al. (2006). Radial velocities associated with these bubbles are $v_{\text{LSR}} = 24.0 \text{ km s}^{-1}$ for N115 (Watson et al. 2010)

and $v_{\text{LSR}} = 42.8 \text{ km s}^{-1}$ for N117 (Watson et al. 2003)¹; these velocities belong to the (molecular or ionized) gas associated with these bubbles.

There are two large radio objects in the vicinity of the bubbles: SNR G54.4-0.3 and a radio loop G053.9+0.2 (see Fig. 3, the left panel). SNR G54.4-0.3 was studied by Junkes et al. (1992a) and found to be associated with the CO gas at around $v_{\text{LSR}} = 40.0 \text{ km s}^{-1}$. The loop G053.9+0.2 was studied by Leahy et al. (2008) and was found to be related to an IR shell, which itself was connected to CO emission and HII regions with velocities around $v_{\text{LSR}} = 40.0 \text{ km s}^{-1}$. The CO and the HII regions in the vicinity of the loop G053.9+0.2 were extensively studied by Xu & Ju (2014) and the connection with IR bubbles N116 and N117 was explicitly claimed (see Fig. 1 for their image of the region).

The pulsar wind nebula, connected with the SNR054.1+0.3 (Green 2009), is projected to the wall of the larger radio loop, but according to Leahy et al. (2008), is not physically associated with it, as it probably lies at a different radial velocity (53 km s^{-1}). This pulsar wind nebula is created by the young pulsar PSR J1930+1852 (the characteristic age of the pulsar is 2900 yr).

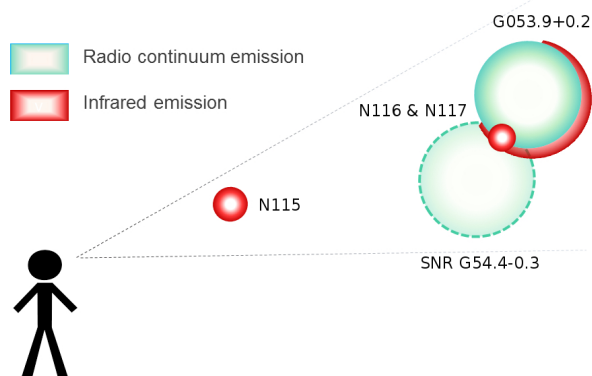


Fig. 1. A cartoon of the region surrounding G053.9+00.2 according to Xu & Ju (2014): N116+117 connected to the radio loop G053.9+0.2 and the independent N115 and SNR G54.4-0.3.

2. Data and methods

2.1. Data

For our study, we use the following surveys:

- Spitzer-GLIMPSE survey (Galactic Legacy Infrared Mid-Plane Survey Extraordinaire, Benjamin et al. 2003) with a pixel resolution of $1.2''$. We use the $8.0 \mu\text{m}$ filter.
- VGPS (VLA Galactic Plane Survey, Stil et al. 2006) for the HI and radio continuum data. The angular resolution is $1'$, the channel width for HI is 1.2 km/s .
- GRS (Galactic Ring Survey, Jackson et al. 2006) for CO data. The angular resolution is $46'$, the channel width is 0.2 km/s .

¹ Watson et al. (2010) gives the $v_{\text{LSR}} = 18.7 \text{ km s}^{-1}$ for N117, but the cited value is not found in the given reference — as also noted by Xu & Ju (2014) — and therefore we disregard it.

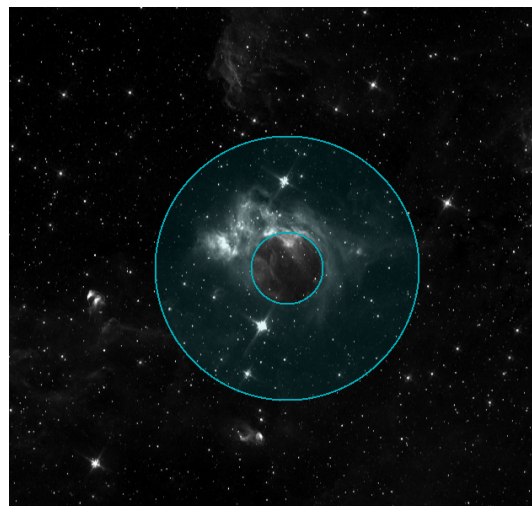


Fig. 2. The example of a mask for a case of the bubble F (= IR bubble N115).

We searched the surroundings of known IR bubbles N115, N116 and N117. N116 and N117 are listed separately in Churchwell et al. (2006) but based on their appearance and in accordance with HI, CO and radio continuum observations we consider them to be one physical entity (see also the discussion in Section 3.1). We manually constructed a mask (see the example in Fig. 2) based on the appearance of bubbles in the IR data (using the ds9 tool – Smithsonian Astrophysical Observatory (2000)) — basically a ring — and applied it to the HI and CO data. We searched for regions with significant contrast between the temperature of the ring and temperatures inside and outside the ring. We also applied masks, which were 25 percent wider or narrower than the original mask. However, the results did not differ significantly from each other. Such discovered regions were then inspected visually to confirm the connection between the infrared and HI or CO structures. Even though there are previous proposed connections between studied IR bubbles and the CO emission (see the subsection 1.2 in the Introduction), we do not use this a priori knowledge in our search to see, if we will come to the same conclusions. HI data, to our best knowledge, were not studied in the connection with these bubbles.

As another source of information about the distribution of the cold phase of the interstellar medium we use “BGPS clumps” from Dunham et al. (2011). These are sources detected in the Bolocam Galactic Plane Survey (1.1 mm), which are also detected in the NH_3 line by the Green Bank Telescope. Diameters of these structures lie in the range $33''$ and $5.9'$, but the objects in our studied region are smaller than $2.1'$, which correspond to linear sizes between 0.3 pc and 3 pc for our assumed distances. These sizes lie in the interval of sizes given for clumps by Bergin & Tafalla (2007), i.e. objects smaller than clouds and larger than cores. That is why we adopt the name “BGPS clumps” for these tracers of the dense gas.

2.2. Determination of bubbles properties

Knowing the line-of-sight velocity of a bubble we compute its kinematic distance using the flat rotation curve ($R_\odot = 8.5 \text{ kpc}$, $V_\odot = 220 \text{ km s}^{-1}$).

We derive masses of its atomic and molecular component by using formulas from Rohlfs & Wilson (1996). The neutral

hydrogen column density N_{HI} is derived by:

$$N_{\text{HI}} = 1.8 \times 10^{18} \int T_b dv, \quad (1)$$

where T_b is observed brightness temperature of the HI line. The ^{13}CO column density $N_{^{13}\text{CO}}$ is derived by:

$$N_{^{13}\text{CO}} = 2.6 \times 10^{14} \frac{T_{\text{ex}}}{1 - e^{-T_0/T_{\text{ex}}}} \int \tau(v) dv, \quad (2)$$

where T_{ex} is the excitation temperature, which we assume to be 30 K. T_0 for the frequency 110 GHz of the ^{13}CO ($J = 1 - 0$) is 5.3 K. τ is the optical depth derived by the formula:

$$\tau = -\ln \left[1 - \frac{T_b}{T_0} \left[(e^{T_0/T_{\text{ex}}} - 1)^{-1} - (e^{T_0/T_{\text{CMB}}} - 1)^{-1} \right]^{-1} \right], \quad (3)$$

where T_b is the observed brightness temperature of the CO line and T_{CMB} is the cosmic microwave background temperature of 2.7 K. The GRS survey provides maps of the antenna temperature T_A , which has to be converted to the brightness temperature: $T_b = T_A/\eta_{\text{MB}}$, where $\eta_{\text{MB}} = 0.48$.

Using the sizes and column densities we calculate the original density of the medium, into which the bubble expanded. We give results for HI and CO separately.

Knowing the radius r of the bubble and its expansion velocity v_{exp} we can compute its age (Chevalier 1994) t_{exp} as

$$t_{\text{exp}} = \alpha \frac{r}{v_{\text{exp}}}, \quad (4)$$

where $\alpha = 3/5$ applies to bubbles created by a continuous supply of energy from an OB association and $\alpha = 2/5$ to bubbles created by one-time abrupt supernova explosion.

We estimate the total energy input E_{tot} to create the bubble using the Chevalier's formula:

$$\frac{E_{\text{tot}}}{\text{erg}} = 5.3 \times 10^{43} \left(\frac{n}{\text{cm}^{-3}} \right)^{1.12} \left(\frac{r}{\text{pc}} \right)^{3.12} \left(\frac{v_{\text{exp}}}{\text{km/s}} \right)^{1.40}, \quad (5)$$

where n is the derived density in the vicinity of the bubble.

We compare our estimates of energies and ages with stellar models (Schaller et al. 1992) and try to derive the masses of the progenitor stars.

3. Results

Based on analysis of both the HI and CO data we find, in agreement with previous observations, that infrared bubbles N115 and N116+117 lie at different radial velocities and thus at different distances from us. The bubble N116+117, which has the radial velocity around $v_{\text{lsr}} \simeq 40 \text{ km s}^{-1}$, was assumed to be connected to a larger radio continuum bubble (Xu & Ju 2014). We confirm this and also believe, that it is in fact connected to both radio bubbles seen in this direction. We also find that the bubble N115 ($v_{\text{lsr}} \simeq 24 \text{ km s}^{-1}$) has two larger accompanying bubbles best visible in the HI gas.

The radial velocity of 40 km s^{-1} is close to the terminal velocity in the direction of $l = 54^\circ$ and therefore we place the N116+117 system at the tangential point corresponding to the distance of 5 kpc. The velocity 24 km s^{-1} has both the near and far kinematic distances. In accordance with most other authors (and also for reasons given below) we adopt the near distance as

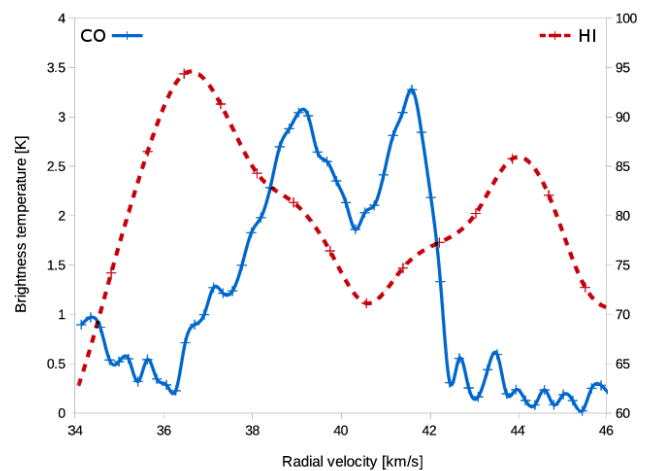


Fig. 4. The CO (a solid blue line, the left y-axis) and HI (a dashed red line, the right y-axis) spectrum of the bubble C (the background system). The HI spectrum is taken at the position (54.087° , -0.068°), the CO spectrum at the position (54.123° , -0.103°).

more appropriate. Therefore we call the system with the radial velocity of 24 km s^{-1} , containing the infrared bubble N115, as the foreground system, and the system with the radial velocity of 40 km s^{-1} as the background system.

Table 1 gives an overview of the bubbles identified in the area, their positions and alternate names. Table 2 summarizes their dimensions, derived masses and densities (Eqs. 1-3), and energies involved in their creation (Eq. 5)

3.1. Background system

The background system, centered around the IR bubble N116+117 at the radial velocity of $\sim 40 \text{ km s}^{-1}$, lies at the distance of approximately 5 kpc. For the purposes of the description we will name the larger bubbles of this system as A and B, and the smaller bubble (which is coincident with the IR bubble N116+117) as C. The diameter of the small bubble C in Figures (and its typical size in all studied spectral regions) is $5'$, diameters of A and B are $39'$ and $45'$, respectively. In linear dimensions it corresponds to 7 pc (C) and 56 or 65 pc (A and B).

In the infrared emission ($8\mu\text{m}$) the small bubble C is described by Churchwell et al. (2006) as two bipolar bubbles, one incomplete (N116) and one closed (N117), see Fig. 3, the right part. Also the larger bubble A is observable in this spectral region as an incomplete ring surrounding a region devoid of any extended emission (see Fig. 3, the upper panel the left part; the brightest emission in the wall of A rightward from C does not belong to this system, it is N115 and belongs to the foreground system). The bubble B has no clear counterpart in the IR region.

All three bubbles are visible in the radio continuum image. C is the brightest one, with the radio continuum filling the interior of the infrared structure. A is visible as the closed irregular ring. B forms the incomplete but well defined spherical ring (Fig. 3, the second panel, the left part).

The bubble best visible in the HI emission is small C. It is a small hole, which is filled by the radio continuum emission (Fig. 3, the right half). The hole is surrounded by a fragmented denser wall. If the structure expands at all, its expansion velocity is small, around 4 km s^{-1} . Bubbles A and B are not visible, or at least not visible with a sufficient credibility. The region is complex and full of arcs, loops and holes, and therefore one can

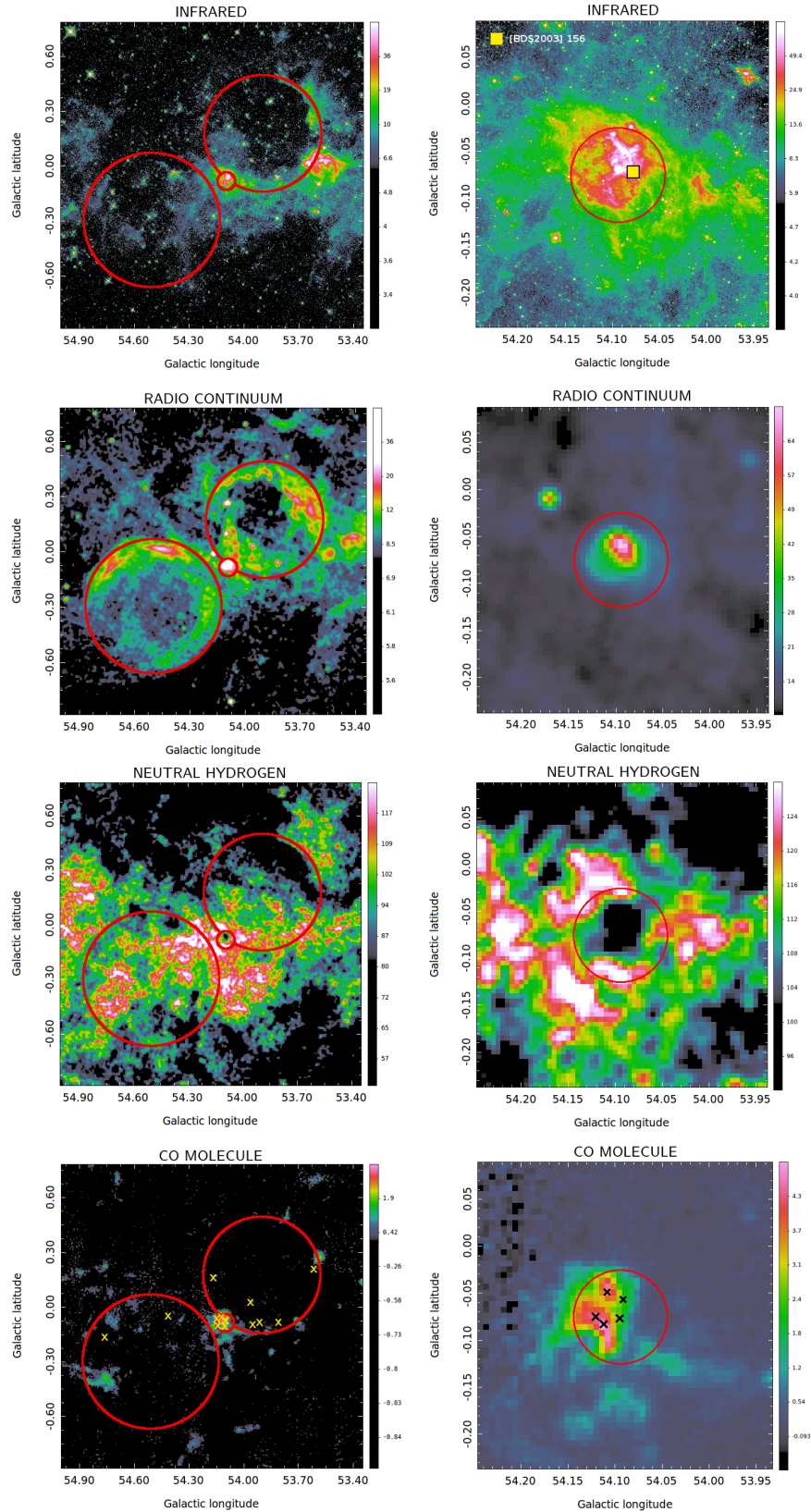


Fig. 3. The multiwavelength image of the background system (left: the total system, right: the small central region). Positions of bubbles A (upper right), B (lower left) and C (small in the middle) are overlaid. The HI is summed over the velocity interval: $38.9 \text{ km s}^{-1} < v_{LSR} < 42.2 \text{ km s}^{-1}$ (left) and $39.8 \text{ km s}^{-1} < v_{LSR} < 42.2 \text{ km s}^{-1}$ (right), the CO over the interval: $38.6 \text{ km s}^{-1} < v_{LSR} < 41.6 \text{ km s}^{-1}$ (left) and $38.4 \text{ km s}^{-1} < v_{LSR} < 41.8 \text{ km s}^{-1}$ (right). Crosses in the CO pictures belong to the BGPS clumps found at the corresponding velocity intervals.

Table 1. Measured properties of the studied bubbles: positions, radial velocities and diameters, together with wavelengths, where the bubble is nicely seen or where it was previously detected and described. 'B' and 'F' stands for the background or foreground system.

Name	l [deg]	b [deg]	v_r [km/s]	d [arcmin]	Prominent data	System	Alternative name
Bubble A	53.885	+0.180	41.4	39	radio continuum	B	Leahy's large-scale bubble
Bubble B	54.498	-0.303	40.0	45	radio continuum	B	SNR G54.4-00.3
Bubble C	54.089	-0.087	40.0	5	IR emission	B	N116 & N117
Bubble D	53.821	+0.302	25.0	78	HI line	F	-
Bubble E	53.257	-0.419	24.9	54	HI line	F	-
Bubble F	53.556	-0.014	24.1	13	IR emission	F	N115

Table 2. Properties of identified bubbles. R is the mean radius, v_{exp} is the expansion velocity, M_{HI} is the mass of the bubble in HI, M_{H_2} is the molecular mass from, n is the density of the medium into which the bubble was expanding (derived from HI and CO), E is the energy needed to create the bubble. The bubble B is the special case: its expansion velocity does not come from our measurements and its age is likely to be higher (see the Section 3.1.1).

Bubble	R [pc]	v_{exp} [kms $^{-1}$]	M_{HI} [M_\odot]	M_{H_2} [M_\odot]	n_{HI} [cm $^{-3}$]	n_{H_2} [cm $^{-3}$]	E [10^{50} erg]	age [Myr]
A	28	7	$2.4 \cdot 10^4$	$1.4 \cdot 10^5$	13	31	4.0	2.7
B	32	50 *	$1.2 \cdot 10^4$	$1.4 \cdot 10^5$	3.4	19	26.0	0.3*
C	4	4	360	$3.4 \cdot 10^4$	160	$7.5 \cdot 10^3$	> 0.028	0.5
D	23	5	$2.4 \cdot 10^3$	$5.6 \cdot 10^4$	1.8	20	0.19	3.6
E	17	6	$2.1 \cdot 10^3$	$3.0 \cdot 10^4$	3.9	26	0.21	2.3
F	4	4	130	$1.5 \cdot 10^4$	23	$1.3 \cdot 10^3$	> 0.008	0.6

easily see things which are not there. However, there is a suspicious coincidence of the HI deficiency and the radio continuum emission at the upper-right part of the wall in the bubble A and the HI emission just next to this deficiency, corresponding to the IR emission (Fig. 3, upper three panels in the left). We are unable to measure the expansion velocity of the bubble B, therefore we take it from Park et al. (2013), and we estimate the expansion velocity of A based on the mentioned structure.

The brightest CO emission at around $\sim 40 \text{ kms}^{-1}$ lies very near to the bubble C. The bubble itself does not lie in the centre of the emission but at its edge (Fig. 3). Interestingly looking CO arcs protrude from this bright region (they merge at the bubble C). They have the general direction of the radio continuum emission. Walls of all three bubbles contain cold molecular clumps (BGPS clumps = crosses in the lowest panels in Fig. 3). Fig. 4 shows the spectrum through the centre of the bubble C (HI) and through the brightest CO emission inside the bubble (CO). HI expansion velocity is larger than the CO expansion velocity, which we mostly ascribe to the off-centre position of the CO spectrum.

On the whole it looks like we observe two colliding bubbles. These bubbles (A and B) are seen as rings of the warm ionized gas. The bubbles probably interact with the neutral gas around them, as seen in the distribution of cold molecular gas (in walls) and also partly in the IR emission of the heated dust and the HI emission of the atomic gas. Linear radii of these bubbles are around 30 pc . In the region, where these two bubbles collide, there is another, much smaller bubble, which is compact, with walls made from the neutral gas and partly traced also by the molecular gas. This small bubble (C) is filled with the ionized gas.

3.1.1. Properties of bubbles A, B and C

Using Eqs. 1-5 we calculate masses of individual bubbles (around $10^5 M_\odot$ for A and B and about a third for C), energies needed to create the structures (using the density n_{HI} derived from the HI measurements, which means, that this number is

a lower limit for the energy, especially for the small bubble C where the volume filling factor of the dense molecular gas is quite high) and their ages (2 Myr for A and 0.5 Myr for C). We do not measure the expansion velocity of B; if we take the value from Park et al. (2013) we get the age of 0.3 Myr. This age is too young for the bubble B to be able to create the small bubble C by the collision with the bubble A. However, from the Junkes et al. (1992b) and Park et al. (2013) it seems plausible, that this supernova evolves inside the stellar wind bubble (and still resides inside it) and therefore the older stellar bubble is the one, which collides with the bubble A.

All calculated values can be found in the Table 2. Energies involved in the creation of bubbles A and B are quite high ($\sim 4 \times 10^{50}$ erg for A and $\sim 2.6 \times 10^{51}$ erg for B). This is not surprising for the bubble B, which is the supernova remnant, but even the bubble A is quite energetic. It could be an old supernova remnant (Leahy et al. 2008), but the needed energy could be supplied by stars, but either a very massive star or several less massive would be needed. The bubble C is much less energetic and it can be easily powered by the stellar wind of a star, which is able to ionize its surrounding.

3.2. Foreground system

The foreground system, centered around the IR bubble N115 at the radial velocity of $\sim 24 \text{ kms}^{-1}$, lies at the distance of approximately 2.1 kpc. Looking at the 3rd panels of Fig. 5 we see, that it contains not only the small central bubble, but also two larger ones. We name the larger bubbles of this system as D and E, and the smaller bubble (which is coincident with the IR bubble N115) as F. The diameter of the small bubble F in Figures (and its typical size in all studied spectral regions) is $13'$, diameters of D and E (more precisely, geometrical means of their axes) are 1.3° and 0.9° , respectively. For the near kinematic distance, which is our adopted distance, these values correspond to 8 pc (F), 46 pc (D) and 34 pc (E). At the far kinematic distance (8 kpc) sizes of the larger bubbles D and E would be around 140 pc. Such values are comparable to the thickness of the HI disk,

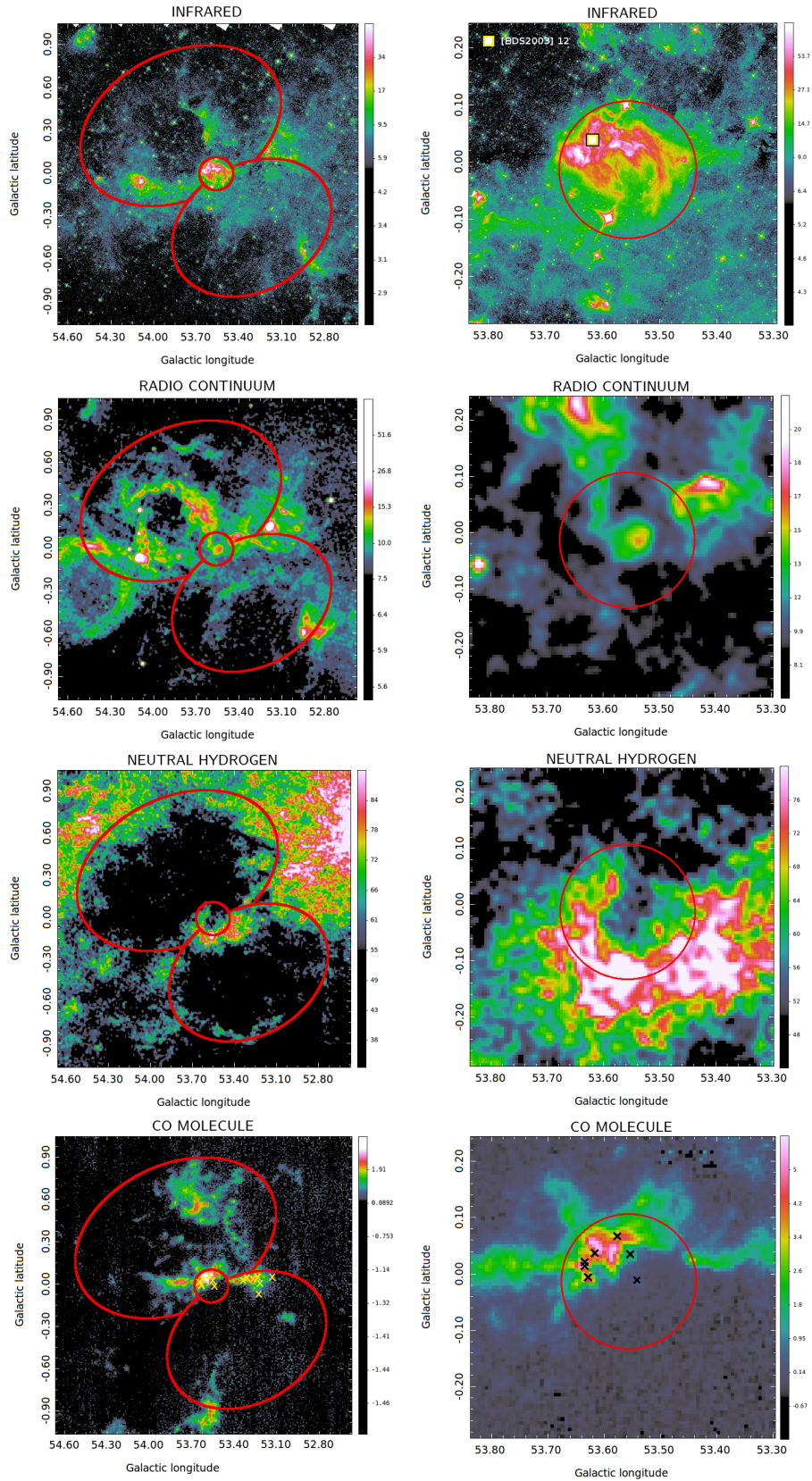


Fig. 5. The multiwavelength image of the foreground system (left: the total system, right: the small central region). Positions of bubbles D (upper left), E (lower right) and F (small in the middle) are overlaid. The HI is summed over the velocity interval: $23.3 \text{ km s}^{-1} < v_{LSR} < 24.9 \text{ km s}^{-1}$ (left) and $23.3 \text{ km s}^{-1} < v_{LSR} < 24.1 \text{ km s}^{-1}$ (right), the CO over the interval: $23.8 \text{ km s}^{-1} < v_{LSR} < 25.0 \text{ km s}^{-1}$ and $23.9 \text{ km s}^{-1} < v_{LSR} < 24.8 \text{ km s}^{-1}$. Crosses in the CO pictures belong to the BGPS clumps found at the corresponding velocity intervals.

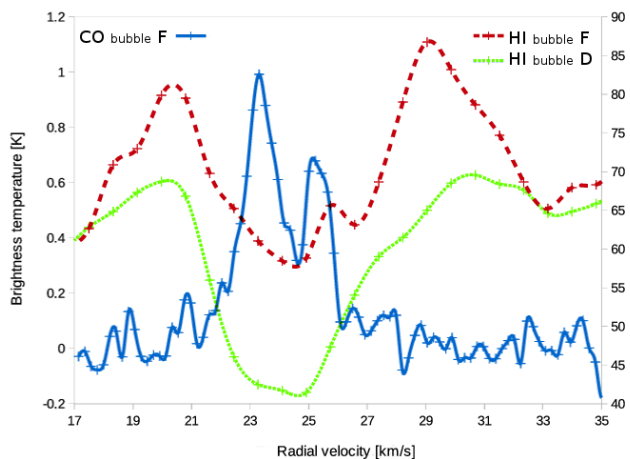


Fig. 6. The CO (a solid blue line, the left y-axis) and HI (a dashed red line, the right y-axis) spectrum of the bubble F (the foreground system). The HI spectrum is taken at the position $(53.573^\circ, -0.059^\circ)$, the CO spectrum at the position $(53.558^\circ, 0.003^\circ)$. The HI spectrum of the bubble D (a dotted green line) is overlaid, its position is $(53.56^\circ, -0.014^\circ)$.

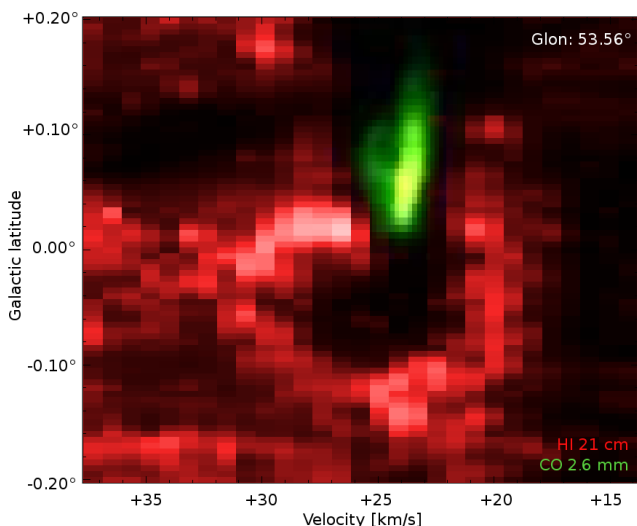


Fig. 7. The latitude-velocity diagram of the bubble F (the foreground system) at $l = 53.56^\circ$. The red color corresponds to the HI emission, the green color to CO.

but we see (Fig. 5, left) that the bubbles are both located inside the disk and are not influenced by the density gradient in the vertical direction. That is the other reason, apart from wanting to be on a safe, lower energetics, side, why we prefer the near kinematic distance.

In the infrared emission ($8\mu\text{m}$) the only clearly visible object is the small bubble F (the IR bubble N115). Churchwell et al. (2006) describes it as a closed ring (see Fig. 5, the upper panel at the right side). A very faint IR emission might be connected to the right-lower wall of the bubble D.

The bubble F is also seen in the radio continuum image. Not very bright emission comes from the interior of the bubble. There might be small and faint regions of the ionized gas along the wall of the bubble D and also along the upper part of the bubble E (Fig. 5).

An object at coordinates $l = 53.19^\circ, b = 0.16^\circ$, visible both in the infrared and radio continuum data, is another IR bubble,

MWP1G053179+001558 (Simpson et al. 2012). According to Bronfman et al. (1996) and Anderson et al. (2009) it lies at the radial velocity $6.6\text{km s}^{-1} \leq v_{lsr} \leq 8.3\text{km s}^{-1}$ and therefore does not belong to our foreground system (and also not to the background system).

The whole foreground system is well visible in the HI emission (see Fig. 5, the 3rd panel, for the channel map at around $v_{lsr} \approx 24\text{km s}^{-1}$ and Fig. 6 for the spectrum through the center of the bubble F). The bubble D is a hole in the HI distribution in this region, i.e. it shows only the region devoid of HI but no prominent walls except where it interacts with E (and where F is located). The bubble E shows, on the contrary, a nice partial wall, or arc, in its lower part.

The brightest CO emission is connected to the small bubble F (see Fig. 5, and also Fig. 7, which is the latitude-velocity diagram of the bubble and which shows how the HI and CO together surround the hot interior of the bubble and supplement each other). Molecular gas in bubbles D and E is located preferentially at the inner edge of the HI structures (it is evident especially in D). One possible scenario is, that the shock wave, which created D or E, was strong enough to push the gas, but not strong enough to completely dissolve it (see Ehlerová & Palouš (2016) for the analysis, how do properties of CO clouds change with the position of clouds inside and outside HI shells). Bubbles F and E contain cold molecular clumps (BGPS clumps = crosses in the lowest panels in Fig. 5), mostly along the wall, where bubbles connect.

The picture which we see in this foreground system resembles the background one: two larger, and therefore probably older, colliding bubbles, with the region of the very recent star formation located in the interacting zone. This zone is the center of activity of the system and is best observable in all studied wavelengths. Unlike in the previously described case, the interacting bubbles seem to be less energetic, as they are not connected to a substantial degree with the ionized gas. This is confirmed by the estimates (Table 2). Ages of interacting bubbles A, B, D and E are similar, but D and E are an order of magnitude less energetic than A.

3.3. Progenitors of bubbles

One (B) of six studied bubbles is a supernova remnant, one (A) might also be one and the rest are created by stellar winds.

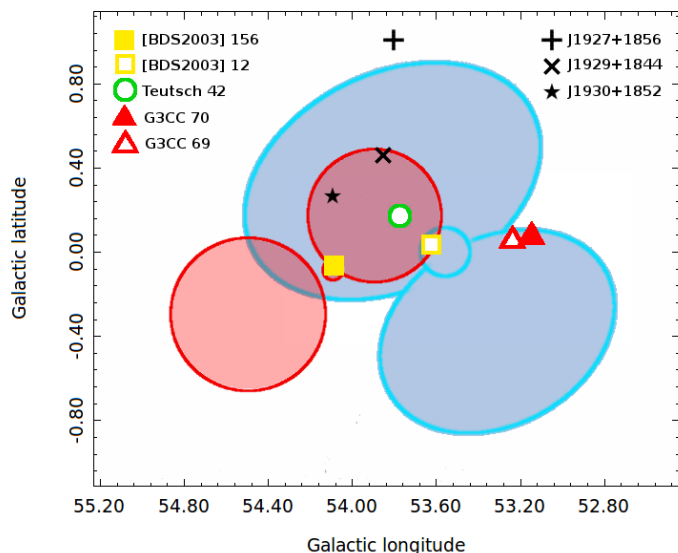
The underlying picture for both systems, the background and the foreground, needs the coeval and cospatial existence of two or more massive stars, which is indicative of the presence of the young cluster.

From Morales et al. (2013) we have selected young (< 100 Myr) clusters in the area: Teutsch 42, [BDS2003] 12 and 156, G3CC 69 and 70. Their positions are shown in the Fig. 8 (together with the schematic positions of bubbles) and given in Table 3. From the spatial distribution it looks like that [BDS2003] 12 is connected to the bubble F (IR bubble N115), [BDS2003] 156 to the bubble C (N116+117), Teutsch 42 to either bubble A or D. G3CC 69 and 70 might be connected to the infrared bubble MWP1G053179+001558 (which does not belong to any of our studied systems). Radial velocities given in Morales et al. (2013) and cited in Table 3 belong to the gas associated with the clusters.

[BDS2003] 156 and 12 are both young clusters still embedded in the gas and dust envelopes (Morales et al. 2013). Their radial velocities correspond to the radial velocities of the bubbles, which the clusters seem to lie in ([BDS2003] 156 in C = N116+117 and [BDS2003] 12 in F = N 115). The first connec-

Table 3. Young clusters in the studied area.

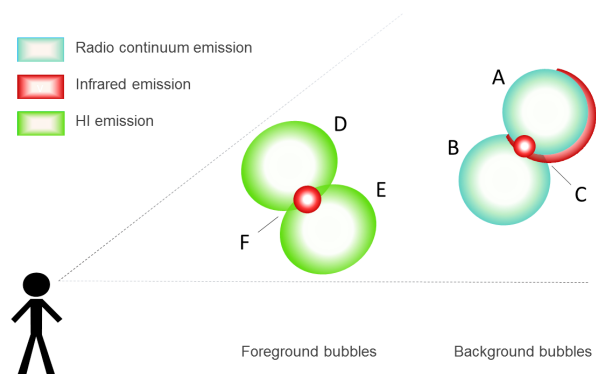
Name	l [deg]	b [deg]	v_{lsr} [km/s]	age [Myr]	Type
G3CC 69	53.147	0.071	22.0		embedded
G3CC 70	53.237	0.056	23.9		partially emb.
BDS2003 12	53.622	0.039	23.7		embedded
Teutsch 42	53.771	0.164	37.7	3	exposed, assoc.
BDS2003 156	54.084	-0.069	39.9		embedded


Fig. 8. A schematic picture of the two systems, background (smaller red one) and foreground (larger blue one) with young clusters and pulsars in the area.

tion is also noted by Morales et al. (2013). The unknown but young age of the cluster and its state of being still embedded in the parental gas satisfies our idea of the star formation recently triggered by the colliding bubbles. The newly formed stars then create and heat the bubbles around them (C and F).

Clusters G3CC 69 and 70, also young and embedded, lie in the projected vicinity of the infrared bubble MWP1G053179+001558. However, the assumed radial velocity of this bubble is around 7 km s^{-1} (see Section 3.2 for references), and they do not seem to be physically connected, as the gas around the clusters has the radial velocity of $\sim 23 \text{ km s}^{-1}$. This velocity is the same as the velocity of the foreground system and therefore if there is any connection, it might be to this system. Still, they are too young to be progenitors of the larger bubbles of the foreground system.

The last cluster in this area (Teutsch 42) is the most studied cluster of them all. There is a wide range of possible distance and age pairs for this object: 1.6 kpc and 30 Myr (Kronberger et al. 2006); 2.0 kpc and 1.3 Myr (Kharchenko et al. 2013); 6.7 kpc and 3 Myr (Morales et al. 2013); and 6.5 kpc and 2-4 Myr (Hanson et al. 2010). The last paper from the list (Hanson et al. 2010) describes photometric and spectroscopic observations of this cluster and the quoted distance is the photometric distance, which the authors claim to be in accordance with the kinematic distance (observed line-of-sight velocities of the brightest members of the cluster are large, greater than or similar to 70 km s^{-1} and therefore the stars are assumed to lie at the tangential point). Teutsch 42 contains a WR star and some O and B stars, its mass is $(4 - 6) \times 10^3 M_{\odot}$. This age and a presence of evolved massive stars makes it a very good candidate for the energy source of the


Fig. 9. A cartoon of the region with all previously known and newly identified bubbles. There are two systems: a foreground system (larger bubbles D and E and a small bubble F connected to the IR bubble N115); and the background system (bubbles A = a radio loop GS053.9+0.2, B = SNR G054.4-0.3 and small C = N116+117).

bubble A of the background system. There is still a discrepancy between measured radial velocities of stars in the cluster and the gas associated with this cluster.

There are two pulsars in the area with suitable distances from the Sun: J1929+1844 (the distance of 5.3 kpc) and J1927+1856 (4.8 kpc), Lorimer et al. (2002). One of them could be ejected from the cluster Teutsch 42, but the probability depends on the distance of the cluster, which is not precisely known. It is not unusual for neutron stars to be expelled from their parental clusters, sometimes with high velocities (see Moyano Loyola & Hurley 2013). Unfortunately, at least one of these pulsars seems to be too old for the proposed young age of the cluster (J1929+1844: 8 Myr, about twice the age of Teutsch 42). The other pulsar, J1927+1856, is younger (2 Myr). But even if none of pulsars and the cluster are correlated, stars of the Teutsch 42 (or similar cluster) are able to produce enough energy to create the bubble A.

Bubble B is the supernova remnant (G54.4-0.3). Its progenitor is unknown.

Bubbles D and E have relatively low energetic demands, compatible with several (one to ten, depending on the mass) B stars.

4. Discussion

Both the foreground and the background system look similar. They are formed by two bubbles with radii around 20–30 pc and ages of a few million years which collide. A younger and smaller ($\sim 4 \text{ pc}$, less than a million years old) bubble lies at the position of the collision. While this small bubble is best seen in the infrared data, it is much better visible at all studied wavelengths (IR, radio continuum, HI, CO) than the larger structures. Fig. 9 shows our

new, more complicated image of the area, where the interacting bubbles are depicted.

Average densities of the ISM, both corresponding to HI and CO, are higher for the smaller shells. For the bubbles with radii around 20 pc, the densities are several H cm^{-3} for HI and several $10 \text{ H}_2 \text{ cm}^{-3}$ for CO. For the smaller bubbles the density is (10-20) times higher for HI and 100 times higher for CO. This is likely the result of the star formation taking place in the densest parts of the ISM, and as the structure created by the massive, energy-releasing star, grows, the ISM becomes less and less dense.

These two systems, though they are similar, differ especially in the amount of energy involved in their creation. The background system, the one in the vicinity of the IR bubble N116+117, is more energetic. Bubble B is a known supernova remnant (Green 2009). Bubble A might also be one: our energy estimates are high enough to be consistent with this hypothesis. But it could also be a more energetic stellar-wind blown bubble. Other bubbles, i.e. the IR bubbles connected to N116+117 and to N115, and the whole foreground system, are probably created by stellar winds or ionizing radiation of massive stars. Energetic requirements, estimated by the Eq. 5 of most of the structures can be fulfilled by one massive star. In the future, these bubbles either merge and create larger structures (if the energy supply is sufficient), or they will soon disappear into undetectability and blend with the surrounding.

There are some young clusters in this area. At least two of them are connected to the studied bubbles: [BDS2003] 156 to a small bubble C (= N116+117) and [BDS2003] 12 to small F (= N 115). Teutsch 42 might be the progenitor of the bubble A (= IR loop GS053.9+0.2). The connection of our studied systems to two young clusters G3CC 69 and 70 and to three young pulsars (J1927+1856, J1929+1844, J1930+1852) in the area is unclear.

4.1. Colliding systems

Perhaps our most interesting finding is that both infrared bubbles (N115 and N116+117) are associated with collisions of larger and older bubbles. While we do not claim, that all IR bubbles are created by collisions, these events must be important in promoting star formation. We therefore propose, that such collision increase the probability of further star formation, probably by squeezing the material and increasing its density.

In addition to the C&C or RDI scenarios, the collision driven "Collect & Collide" triggered star formation process should also be considered.

Acknowledgements. This study has been supported by the Czech Science Foundation grant 209/12/1795 and the MŠMT grant LG14013.

References

- Anderson, L. D., Bania, T. M., Jackson, J. M., et al. 2009, ApJS, 181, 255
 Benjamin, R. A., Churchwell, E., Babler, B. L., et al. 2003, PASP, 115, 953
 Bergin, E. A. & Tafalla, M. 2007, ARA&A, 45, 339
 Bronfman, L., Nyman, L.-A., & May, J. 1996, A&AS, 115, 81
 Chevalier, R. A. 1994, in Supernovae, ed. S. A. Bludman, R. Mochkovitch, & J. Zinn-Justin, 743
 Churchwell, E., Povich, M. S., Allen, D., et al. 2006, ApJ, 649, 759
 Dale, J. E., Haworth, T. J., & Bressert, E. 2015, MNRAS, 450, 1199
 Deharveng, L., Schuller, F., Anderson, L. D., et al. 2010, A&A, 523, A6
 Dunham, M. K., Rosolowsky, E., Evans, II, N. J., Cyganowski, C., & Urquhart, J. S. 2011, ApJ, 741, 110
 Ehlerová, S. & Palouš, J. 2016, A&A, 587, A5
 Green, D. A. 2009, Bulletin of the Astronomical Society of India, 37, 45
 Hanson, M. M., Kurtsev, R., Borissova, J., et al. 2010, A&A, 516, A35

- Jackson, J. M., Rathborne, J. M., Shah, R. Y., et al. 2006, ApJS, 163, 145
 Junkes, N., Fuerst, E., & Reich, W. 1992a, A&AS, 96, 1
 Junkes, N., Fuerst, E., & Reich, W. 1992b, A&A, 261, 289
 Kharchenko, N. V., Piskunov, A. E., Schilbach, E., Röser, S., & Scholz, R.-D. 2013, A&A, 558, A53
 Kronberger, M., Teutsch, P., Alessi, B., et al. 2006, A&A, 447, 921
 Leahy, D. A., Tian, W., & Wang, Q. D. 2008, AJ, 136, 1477
 Lorimer, D. R., Camilo, F., & Xilouris, K. M. 2002, AJ, 123, 1750
 Morales, E. F. E., Wyrowski, F., Schuller, F., & Menten, K. M. 2013, A&A, 560, A76
 Moyano Loyola, G. R. I. & Hurley, J. R. 2013, MNRAS, 434, 2509
 Park, G., Koo, B.-C., Gibson, S. J., et al. 2013, ApJ, 777, 14
 Rohlfs, K. & Wilson, T. L. 1996, Tools of Radio Astronomy
 Schaller, G., Schaerer, D., Meynet, G., & Maeder, A. 1992, A&AS, 96, 269
 Simpson, R. J., Povich, M. S., Kendrew, S., et al. 2012, MNRAS, 424, 2442
 Smithsonian Astrophysical Observatory. 2000, SAOImage DS9: A utility for displaying astronomical images in the X11 window environment, Astrophysics Source Code Library
 Stil, J. M., Taylor, A. R., Dickey, J. M., et al. 2006, AJ, 132, 1158
 Walch, S., Whitworth, A. P., Bisbas, T. G., Hubber, D. A., & Wünsch, R. 2015, MNRAS, 452, 2794
 Watson, C., Araya, E., Sewilo, M., et al. 2003, ApJ, 587, 714
 Watson, C., Hanspal, U., & Mengistu, A. 2010, ApJ, 716, 1478
 Xu, J.-L. & Ju, B.-G. 2014, A&A, 569, A36